Research Square

Preprints are preliminary reports that have not undergone peer review.
They should not be considered conclusive, used to inform clinical practice,
or referenced by the media as validated information.

Active Steering of Material Flow in Large-Scale Bellows Roll Forming via Spatially Modulated Die Friction

Hao Fu

fh@ujs.edu.cn

Jiangsu University School of Mechanical Engineering

Jialin Qu
Hangcheng Zhang
Tianyu Shan
Shuqian Wu
Jingjing Zhang
Hexing Li
Yuyang He
Yanhu Zhang
Jinghu Ji
Yonghong Fu

Research Article

Keywords: Metal bellows, Roll forming, Friction design, Hybrid laser micro-texturing, Material flow control, Wall thickness uniformity

Posted Date: June 30th, 2026

DOI: https://doi.org/10.21203/rs.3.rs-9674254/v1

License: This work is licensed under a Creative Commons Attribution 4.0 International License.
Read Full License

Version of Record: A version of this preprint was published at The International Journal of Advanced Manufacturing Technology on October 2nd, 2026. See the published version at https://doi.org/10.1007/s00170-026-19247-3.

Active Steering of Material Flow in Large-Scale Bellows Roll Forming via Spatially Modulated Die Friction

Hao Fu [a*], Jialin Qu [b], Hangcheng Zhang [b], Tianyu Shan [b], Shuqian Wu [c], Jingjing Zhang [d], Hexing Li[b], Yuyang He [b], Yanhu Zhang [a], Jinghu Ji [b], Yonghong Fu [b]

[a] Institute of Advanced Manufacturing and Modern Equipment Technology, Jiangsu University, Zhenjiang, China

[b] School of Mechanical Engineering, Jiangsu University, Zhenjiang, China

[c] Ewigkeit Precision Technology Co., Ltd, Nantong, China

[d] School of Management, Jiangsu University, Zhenjiang, China

* Corresponding author.

Email address: fh@ujs.edu (Hao Fu)

Abstract: The roll forming process of large-scale metallic bellows has long been plagued by severe wall thinning at the crest. This defect, which fundamentally compromises fatigue life and structural integrity, is exacerbated by the uncontrolled material flow under the uniform friction conditions inherent to conventional tooling. To address this, we propose a novel strategy to actively steer material flow by tailoring spatially modulated friction profiles across the die surfaces. This strategy is implemented through a hybrid laser surface texturing approach: friction-enhancing convex crater-like micro-textures are fabricated on the inner roller to inhibit outward material flow from the wave crest, while friction-reducing concave micro-dimples are applied to the outer roller to promote inward material replenishment from the feeding zone. Guided by friction sensitivity analysis, textures were selectively fabricated only on critical sensitive zones, representing a high-efficiency manufacturing strategy. Experimental validation demonstrates that the textured tooling achieves a targeted material reallocation—strategically sacrificing the non-critical root to reinforce the vulnerable crest—thereby increasing the minimum wall thickness at the wave crest by 7.54% and enhancing overall uniformity by 11.74%. This work presents a synergistic framework integrating friction-enhancing and reducing textures, offering a robust technique for manipulating material flow and establishing a pathway to surpass the precision limits of traditional forming processes.

Keywords: Metal bellows, Roll forming, Friction design, Hybrid laser micro-texturing, Material flow control, Wall thickness uniformity

1. Introduction

Large-scale metallic bellows serve as indispensable flexible components in critical infrastructure and heavy industries, such as petrochemicals, nuclear energy, and marine engineering. These components perform essential functions, including sealing, pressure compensation, and vibration damping[1, 2]. Characterized by high efficiency and cost-effectiveness, roll forming stands as the predominant technique for manufacturing these thin-walled corrugated structures[3, 4]. However, the complex plastic deformation inherent to this process-involving simultaneous bending, stretching,

and compression-presents a persistent challenge: non-uniform wall thickness distribution. Specifically, excessive wall thinning at the wave crests drastically compromises the fatigue resistance and pressure-bearing capacity[5, 6], ultimately inducing premature and catastrophic failures.

To address this critical technical challenge, research efforts have primarily focused on optimizing manufacturing process parameters[7, 8, 9, 10]. However, these approaches lack robustness and fail to fundamentally resolve the inherent imbalance in material flow. Interfacial friction serves as the critical boundary condition that dictates material flow behavior, stress transfer, and final forming quality[11, 12, 13] Far from acting merely as a source of energy dissipation, friction actively modulates the velocity gradient and strain path by altering tangential constraints. Specifically, the magnitude and distribution of friction directly govern forming loads and limits: excessive friction increases flow resistance, causing localized thinning or fracture; conversely, insufficient friction induces instability or uncontrollable springback[14]. Crucially, the requirement for friction exhibits a significant spatial duality[15]: low friction at the flange facilitates material inflow, while high friction at the punch corner induces a Friction Holding Effect to suppress thinning and delay necking[16].

Despite the growing consensus on the criticality of friction optimization, a substantial gap persists between theoretical principles and practical application. The primary impediment lies in the lack of robust engineering strategies to achieve spatially modulated friction profiles on complex die surfaces. On one hand, friction reduction relies heavily on lubrication[17, 18], surface coatings[19, 20], and polishing[21, 22]. While lubrication is ubiquitous, selectively maintaining distinct lubrication states across specific die regions is practically unfeasible. Similarly, advanced coatings like Diamond-Like Carbon (DLC) typically provide uniform low-friction surfaces, inherently lacking spatial selectivity. Polishing offers only marginal friction reduction, and the resulting surface finish tends to deteriorate rapidly under cyclic loading. On the other hand, the challenge of locally enhancing friction is even more formidable. Techniques such as Electrical Discharge Machining (EDM) texturing[23, 24] or shot peening[25, 26] are commonly employed. However, although these methods elevate the nominal friction coefficient, they generate random and stochastic surface topographies, thereby precluding consistent and predictable tribological behavior.

Laser Surface Texturing (LST) is characterized by its high precision, controllability, and versatility, enabling the non-contact fabrication of deterministic micro-features directly onto tool surfaces. For friction reduction, LST typically employs laser ablation to generate arrays of micro-dimples or grooves[27, 28]. In lubricated contacts, these concave features function synergistically: they act as micro-hydrodynamic bearings to generate additional load-carrying capacity and serve as reservoirs to trap wear debris and mitigate starvation. Furthermore, they physically reduce the nominal contact area, thereby collectively lowering the friction coefficient[29, 30]. Conversely, regarding friction enhancement, LST offers unique advantages over traditional stochastic roughening methods by fabricating convex micro-textures with precisely controllable geometries[31]. The formation of such protrusions relies on a melt-dynamics-driven reshaping mechanism: the high-energy

pulsed laser induces instantaneous surface melting, where the melt pool undergoes dynamic flow driven by the coupling of surface tension gradients and recoil pressure, before rapidly solidifying into spherical-cap or crater-like textures[32, 33]. By promoting mechanical interlocking and enhancing the ploughing component of friction, these deterministic textures increase friction in a highly predictable and repeatable manner[34, 35, 36].

In light of these challenges, this paper proposes a zonal friction control strategy based on hybrid laser surface texturing of roll forming dies, specifically targeting the thinning issues in large-diameter metal bellows used in petrochemical applications. By fabricating friction-enhancing convex textures and friction-reducing concave textures on distinct sensitivity zones of the inner and outer rollers, this approach aims to proactively modulate the interfacial friction field. This, in turn, optimizes material flow balance, thereby minimizing excessive wall thinning at the wave crests. The research methodology is structured as follows: First, a finite element model is established to identify critical friction-sensitive zones and derive an optimized heterogeneous friction distribution map. Second, guided by the simulation results, the corresponding hybrid textures are precisely fabricated onto the die surfaces, physically realizing the theoretical friction design. Finally, comparative roll forming experiments between textured and conventional dies are conducted to verify the efficacy of the proposed laser hybrid texturing in improving wall thickness uniformity.

2. Kinematics and the Inherent Thinning Mechanism in Roll Forming

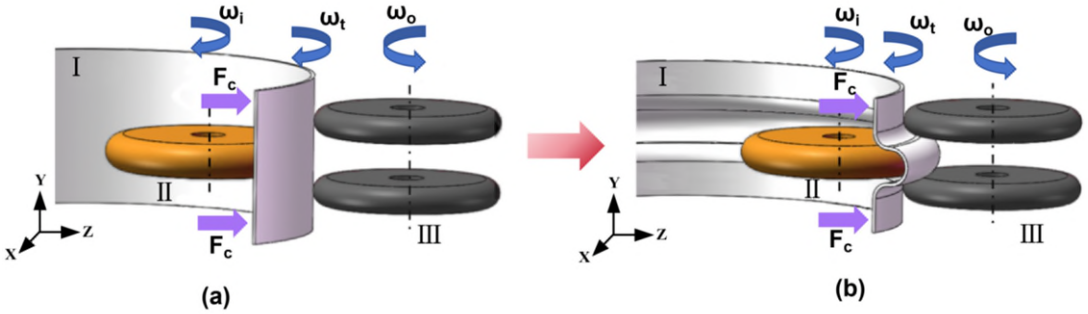


Fig. 1. Kinematic schematic of the incremental roll forming process. The system consists of a tubular blank (I), an inner roller (II), and a pair of outer rollers (III). (a) Initial state: The tubular blank rotates at an angular velocity ω_t kinematically compatible with the inner (ω_i) and outer (ω_o) rollers. A low-magnitude constraint force, F_c, is applied at the free edge to suppress geometric instabilities such as warping and radial run-out. (b) Forming state: The inner roller's radial feed motion progressively deforms the blank, inducing an axial translation of the workpiece to feed the forming zone. Note that the blank and inner roller rotate in the same direction, opposing the rotation of the outer roller.

The roll forming of large-diameter, thin-walled metal bellows is an incremental forming process that progressively shapes a cylindrical tube into a corrugated profile via localized plastic deformation. The process kinematics, illustrated in Fig. 1, are governed by the synchronized rotation of the workpiece and a set of profiled rollers, coupled with a continuous radial feed motion. As the inner roller penetrates the blank

wall, material is forced into the die cavity defined by the outer rollers. Upon completion of a single convolution, the workpiece is indexed axially to the next position, and the cycle is repeated.

From a continuum mechanics perspective, the material at the crest apex—the critical forming zone—is subjected to a severe biaxial tensile stress state. The forced expansion of the tube diameter induces a significant circumferential hoop stress (σ_θ), while the need to draw material from the undeformed flanges generates a meridional tensile stress (σ_ϕ). According to the Levy-Mises flow rule for plastic deformation, the thickness strain rate is proportional to the sum of the principal stresses;

$$\dot{\epsilon}\, t \propto -\left(\sigma_\theta + \sigma_\phi\right) \tag{1}$$

Since both σ_θ and σ_ϕ are tensile (positive) in the crest region, Eq. (1) dictates that the thickness strain rate is inherently negative, rendering wall thinning an inevitable consequence of the process.

The magnitude of this thinning is critically modulated by the interfacial frictional landscape, whose effects exhibit a fundamental duality. At the outer roller interface, the axial material velocity (v_a) required for replenishment is inversely proportional to the total drawing resistance, which includes the frictional drag (τ_0). This relationship can be expressed as:

$$v_a \propto \left(R_{plastic} + R_{friction}(\tau_0)\right)^{-1} \tag{2}$$

where $R_{plastic}$ represents the intrinsic plastic deformation resistance and $R_{friction}$ is the component of resistance arising from friction. High friction at the outer interface increases $R_{friction}$, thereby impeding the compensatory inflow (v_a) and intensifying the meridional tension (σ_ϕ). Conversely, at the inner roller interface, a higher frictional shear stress (τ_i) introduces a resistive force that directly opposes the material's outflow from the crest, thereby preserving thickness. This reveals that friction can either hinder material replenishment or restrain detrimental thinning, depending on its spatial location. A systematic investigation of this dual role is therefore essential for optimizing the material flow of the workpiece.

3. Numerical Investigation of Spatially-Variant Frictional Effects

While the analytical model in Chapter 2 provided a clear hypothesis regarding the opposing effects of friction, it cannot capture the complex, nonlinear interactions inherent to the forming process. Therefore, to deconstruct the sensitivity of wall thickness distribution to localized frictional variations, a comprehensive numerical investigation was conducted.

3.1. Finite Element Model

To systematically investigate and quantify the dual mechanism of friction as hypothesized in Chapter 2, a high-fidelity 3D finite element (FE) model was developed in ABAQUS/Explicit. The model configuration, including key dimensions and meshing

strategy, is detailed in Fig. 2.

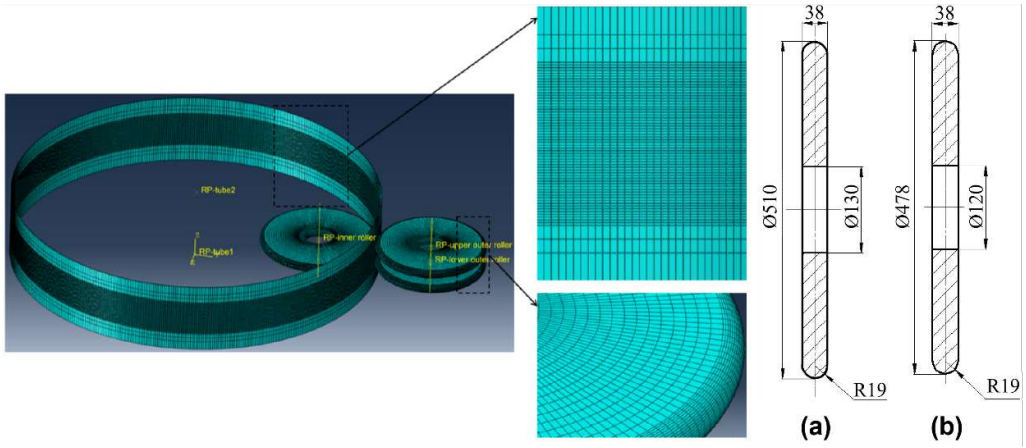


Fig. 2. Configuration and meshing strategy of the finite element model. The main view shows the overall assembly. A graded mesh was applied to the tubular blank to refine the central forming zone. Similarly, the meshes on the rollers were refined at the radiused contact regions to ensure accurate pressure calculation. Insets (a) and (b) provide the detailed geometric dimensions of the inner and outer rollers, respectively.

The model consists of a deformable tubular blank and a set of discrete rigid rollers. The blank was modeled with an initial outer diameter of 1600 mm and a wall thickness of 0.8 mm. The key geometric parameters of the inner and outer rollers are specified in Fig. 2. The initial axial clearance between the inner and outer rollers was set to 0.8 mm. A non-uniform meshing strategy was employed for computational efficiency. The tubular blank was discretized using 4-node general-purpose shell elements with reduced integration (S4R), a choice well-suited for analyses involving finite membrane strains. A graded mesh was applied, with a refined element size of 1.0 mm in the central forming zone, transitioning to 4.0 mm at the free edges. The rollers were discretized using 8-node linear brick elements (C3D8R). To ensure an accurate representation of the contact pressure distribution, the mesh in their radiused contact regions was significantly refined to an element size of approximately 0.5 mm.The material of the tubular blank was SUS304 stainless steel. Its mechanical behavior was described by a rate-independent J2 plasticity model with isotropic hardening, a standard approach for modeling ductile metals under quasi-static conditions. The key elastic properties and the initial yield strength are summarized in Table 1. The plastic hardening behavior, which is critical for accurately predicting material flow, was defined by the true stress-plastic strain curve obtained from uniaxial tensile tests (Fig. 3). This curve was input into the model as a tabular data set.

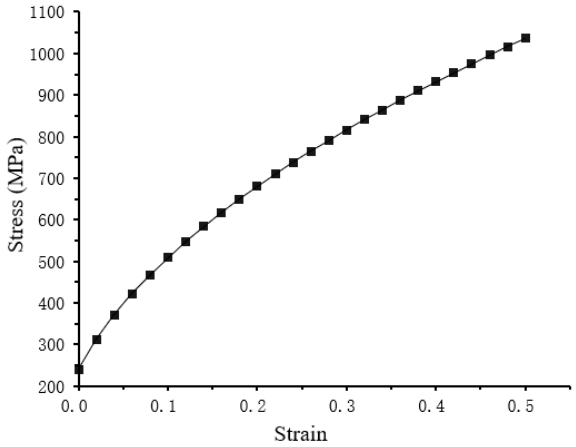


Fig. 3. True stress vs. true plastic strain curve for SUS304.

Table.1 Mechanical properties of SUS304 stainless steel used in the FE model.

Young's Modulus(GPa)	Poisson's Ratio	Density(g/cm^3)	Initial Yield Strength(MPa)
207	0.28	7.83	239.48

The model incorporates realistic kinematic constraints and contact interactions to faithfully replicate the actual industrial manufacturing scenario. The tubular blank was defined as the active driving component, subjected to a prescribed constant angular velocity (ω_t) of 1.5 rad/s as the primary source of rotational motion. To simulate the function of a rotating blank holder and mitigate geometric instability at the free end, a low radial pressure of 2MPa was applied to a 10 mm-wide circumferential element band. Conversely, both the inner and outer rollers were modeled as freely rotating (passive) bodies, driven solely by the frictional contact with the rotating blank. The forming process was actuated by imposing a radial feed rate of 0.3 mm/s on the inner roller, reaching a total feed depth of 50 mm. Contact between all components was managed using the general contact algorithm in ABAQUS/Explicit with a penalty-based formulation. The tangential behavior was governed by an isotropic Coulomb friction model. For the baseline analysis, a uniform friction coefficient of $\mu = 0.1$ was assumed for all interactions, a value representative of the sliding friction coefficient under lubricated cold forming conditions[38] .

3.2. Zonal Partitioning and Parametric Study Scheme

To deconstruct the complex, spatially-dependent role of friction, the active contact surfaces of the rollers were partitioned into distinct zones based on their geometric features and functional roles during forming (Fig. 4). This zonal decomposition provides a structured framework to conduct a one-factor-at-a-time sensitivity analysis. The contact surfaces of the inner and outer rollers were each partitioned into three zones (A-F), as detailed in Table 2. These zones correspond to the key forming regions: the root-contact zone (A), the crest-forming zone (F), and the sidewall zones (B, C, D, E).

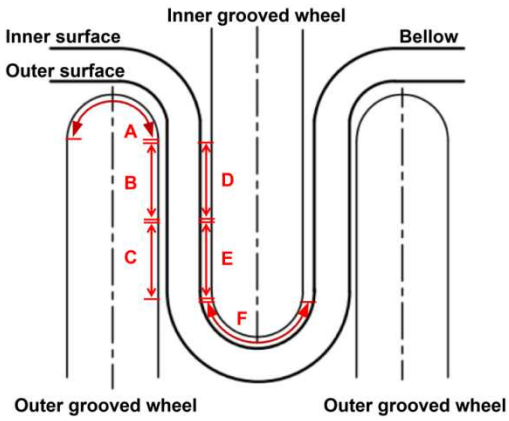


Fig. 4. Zonal partitioning of the active roller-workpiece contact interface. The active contact surfaces of the outer roller and inner roller were partitioned into three zones each (A-C and D-F, respectively) for the parametric study. Zone A corresponds to the root-contact region, Zone D to the crest-forming region, and the remaining zones to the sidewalls.

Table 2. Definition and functional description of the partitioned friction zones on the roller surfaces.

Zone	Roller	Location / Geometry	Primary Function in Forming
A	Outer	Upper semi-circular profile	Shapes the bellow's root; Primary material entry region.
B	Outer	Upper half of the straight section	Guides material flow along the sidewall.
C	Outer	Lower half of the straight section	Finalizes the shape of the outer sidewall.
D	Inner	Upper half of the straight section	Finalizes the shape of the inner sidewall.
E	Inner	Lower half of the straight section	Guides material flow along the inner sidewall.
F	Inner	Lower semi-circular profile	Shapes the bellow's crest; Primary deformation zone.

To systematically investigate the influence of different friction coefficients in each individual region on formability, a systematic parametric study was designed and carried out through numerical simulation. In this approach, the coefficient of friction (COF) for a single target zone was varied across six discrete levels (0.03, 0.07, 0.10, 0.13, 0.16, and 0.20), while the COF in the other five zones was maintained at the baseline value of μ=0.1. To quantitatively evaluate the forming quality, two key metrics were monitored: the minimum wall thickness at the crest (t_{min}), which represents the most critical defect, and the overall wall thickness uniformity index (U), defined as:

$$U = \frac{t_{min}}{t_{max}} \tag{3}$$

where t_{max} is the maximum wall thickness observed in the formed profile. These metrics collectively provide a comprehensive assessment of the material distribution.

3.3. Spatial Sensitivity Analysis and Zonal Classification of Friction Effects

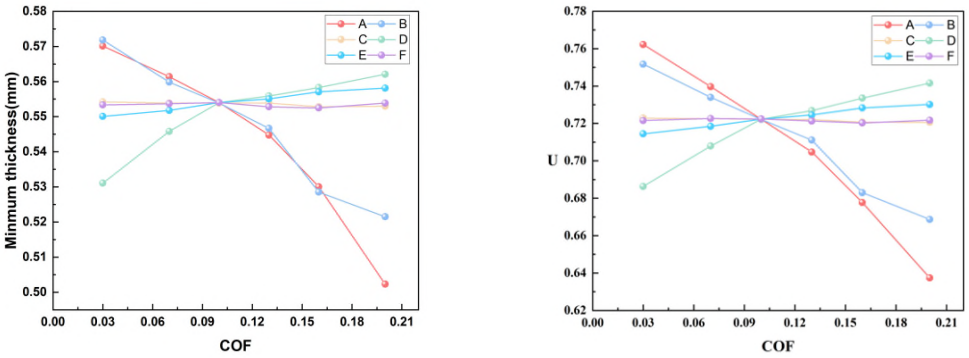


Fig. 5. Sensitivity of forming quality metrics to zonal friction variations.The influence of the COF in each of the six zones (A-F) on (a) the minimum crest thickness (t_{min}) and (b) the wall thickness uniformity index (U).

The results of the parametric study, presented in Fig. 5, reveal a pronounced and highly heterogeneous sensitivity of the forming quality to localized frictional variations. Based on their consistent influence on both the minimum crest thickness (t_{min}) and the uniformity index (U), the roller contact zones can be definitively classified into three functionally distinct categories: beneficial, detrimental, and insensitive.

The most significant positive influence is exerted by the inner roller's crest-forming zones (E and F). As shown in the figures, increasing the COF in these regions leads to a monotonic improvement in both t_{min} and U. This effect is attributed to an enhanced restraining force at the primary deformation site, which effectively counteracts the material's tendency to flow out from the thinning crest. In particular, Region F exhibited the highest sensitivity. Increasing its COF from 0.03 to 0.20 raises t_{min} by approximately 5.8% (from 0.531 to 0.562) and increases U by about 8.5% (from 0.686 to 0.744). The sensitivity ranking is consistently F>E, as Zone F, being the leading contact region with the largest relative slip, has the most dominant impact on material restraint.

Conversely, the outer roller's root-contact zones (A and B) exhibit a strong detrimental effect. Increasing the COF in these regions causes a monotonic degradation in forming quality. This is a direct consequence of increased drawing resistance, which impedes the necessary compensatory material flow from the flange regions to the crest. The effect is most critical in Zone A, where increasing the COF from 0.03 to 0.20 reduces t_{min} by roughly 12% (from 0.57 to 0.502) and causes U to plummet by over 16% (from 0.762 to 0.637). The sensitivity to this negative impact is unambiguously A>B, as Zone A constitutes the primary entry point for material replenishment.

A critical finding is the negligible influence of the outermost sidewall zones (C and D). The response curves for these two zones are nearly flat, indicating their insensitivity

to frictional changes. This is because these zones engage late in the forming sequence when the corrugation profile is nearly complete and relative slip is minimal. This insensitivity provides a crucial insight for manufacturing efficiency, suggesting that surface modification efforts can be strategically focused only on the sensitive zones (A, B, E, F).

In conclusion, this spatial sensitivity analysis establishes a set of guiding principles for functional friction design. First, it articulates a differential regulation strategy: implementing friction enhancement in the inner roller zones (E/F) to reinforce material anchoring, while applying friction reduction in the outer roller zones (A/B) to facilitate material replenishment. Second, it constructs a hierarchical classification system based on sensitivity: defining Zones F and A as Primary Sensitive, Zones E and B as Secondary Sensitive, and Zones C and D as Insensitive. This stratification not only elucidates the core drivers of material flow but also implies a cost-effective manufacturing strategy of focusing on the critical while simplifying the insensitive. These findings serve as the theoretical basis for the optimization design and experimental implementation detailed in the subsequent chapter.

4. Optimization Design and Experimental Implementation of Hybrid Textured Rollers

While the preceding chapter identified the critical friction zones and their required effects, it did not specify the optimal friction magnitudes or the means of their physical implementation. Therefore, this chapter is dedicated to the numerical optimization of the friction map and its subsequent engineering realization via hybrid laser texturing.

4.1. Optimization of Frictional Characteristics on Die Surfaces

The primary optimization objective is to identify the specific combination of friction coefficients across the four sensitive zones (A, B, E, and F) that simultaneously enhances the minimum crest thickness (t_{min}) and the wall thickness uniformity index (U). To efficiently explore this high-dimensional parameter space, the Uniform Design (UD) method was adopted. The core advantage of UD lies in its mathematical ability to minimize the discrepancy of design points. This ensures that the simulation trials are scattered uniformly across the design space, allowing for a comprehensive assessment of the system's response with a minimal number of experiments.

For the beneficial zones (E and F) on the inner roller, the friction coefficient was discretized into 10 levels within the high-friction domain of [0.100, 0.244] (step size: 0.016). Conversely, for the detrimental zones (A and B) on the outer roller, 10 levels were defined within the low-friction domain of [0.028, 0.100] (step size: 0.008). The friction in the insensitive zones (C and D) was fixed at the baseline value of $\mu = 0.1$. A uniform design table was utilized to generate an experimental plan consisting of 10 simulation runs. The specific COF combinations are detailed in Table 3.

Table 3. Experimental plan based on uniform design.

Trial No.	A	B	E	F
1	0.028	0.044	0.148	0.164
2	0.036	0.068	0.212	0.244

3	0.044	0.092	0.100	0.148
4	0.052	0.028	0.164	0.228
5	0.060	0.052	0.228	0.132
6	0.068	0.076	0.116	0.212
7	0.076	0.100	0.180	0.116
8	0.084	0.036	0.244	0.196
9	0.092	0.060	0.132	0.100
10	0.100	0.084	0.196	0.180

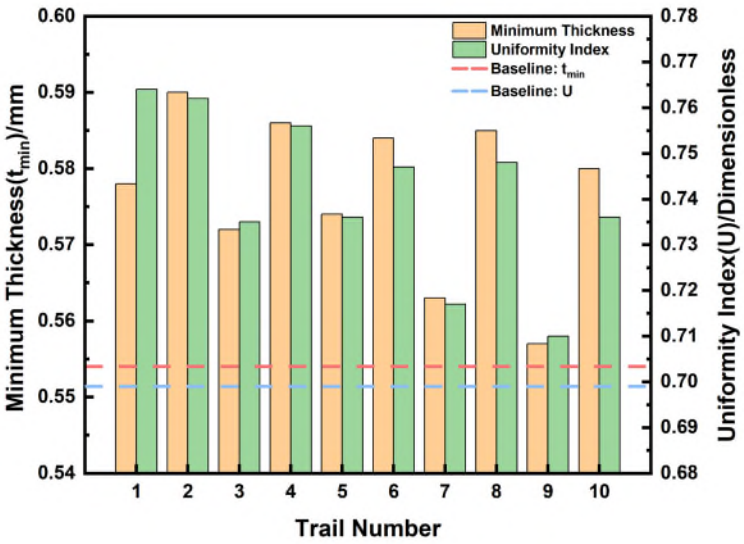


Fig. 6. Comparative assessment of the simulated responses (t_{min} and U).

The simulation results corresponding to Table 3 are visually quantified in Fig. 6. Notably, both t_{min} and U for all optimization trials surpassed the conventional baseline (indicated by the dashed lines), demonstrating the robustness of the friction modulation strategy. Within the design space, Trial No. 1 and Trial No. 2 represent the superior configurations. Specifically, Trial No. 2 achieved the maximum t_{min} (0.59 mm), while Trial No. 1 yielded the highest U value (0.764). The superior thickness retention in Trial No. 2 is attributed to its higher friction coefficients on the inner roller, which exerts a stronger pinning force to inhibit crest thinning. Conversely, the optimal uniformity in Trial No. 1 stems from its rationally minimized friction on the outer roller, which significantly reduces drawing resistance and facilitates global material redistribution. A comparative analysis of these two top-performing configurations reveals a consistent design pattern: the optimized friction distribution aligns closely with the zonal sensitivity hierarchy established in the preceding section:

Inner Roller (Beneficial Friction Zones): The COF in the Primary Sensitive Zone (F) is significantly higher than that in the Secondary Sensitive Zone (E) (i.e., $\mu_F > \mu_E$). This finding strongly substantiates the efficacy of enhancing friction at the wave crest—the most sensitive region—for effective thickness retention.

Outer Roller (Detrimental Friction Zones): Conversely, the COF in the Primary Sensitive Zone (A) is markedly lower than that in the Secondary Sensitive Zone (B)

(i.e., $\mu_A < \mu_B$). This aligns with the design logic of prioritizing resistance minimization in Zone A, which serves as the primary conduit for material flow and is thus most sensitive to drag. In contrast, Zone B demonstrates a higher tolerance for moderately elevated friction levels.

Synthesizing these findings, the quantitative target for physical implementation is established not as a singular parameter set, but as a Gradient Friction Strategy tailored to zonal sensitivity.

4.2. Strategy for Graded Hybrid Texture Design

4.2.1. Texture Selection Strategy

Inner Roller (Friction Enhancement): Convex crater-like micro-textures were selected. Under the high contact stress conditions of plastic forming, the hardened asperities formed by laser remelting significantly enhance mechanical interlocking and micro-ploughing effects at the interface, thereby providing the tangential traction force required for material pinning.

Outer Roller (Friction Reduction): Concave micro-dimple textures were employed. Under the low-speed, heavy-load conditions characteristic of roll forming, these dimples primarily function as micro-reservoirs. They store lubricant and release it under pressure in the deformation zone to induce secondary lubrication. Simultaneously, the dimples entrap wear debris, suppressing abrasive wear and significantly reducing the interfacial coefficient of friction.

4.2.2. Areal Density-Based Gradient Design

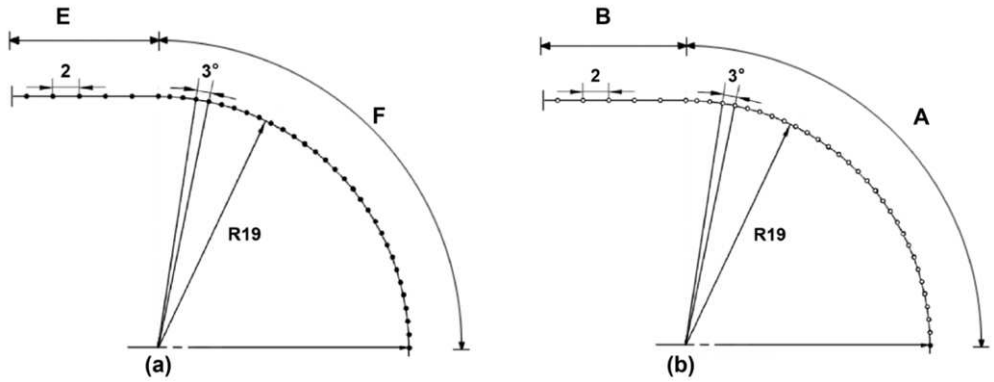


Fig. 7. Schematic representation of the spatially graded texture design applied to the roll forming tooling: (a) Inner roller: Friction-enhancing crater-like textures (denoted by solid circles) applied symmetrically to both flanks. (b) Outer roller: Friction-reducing dimple textures (denoted by hollow circles) applied unilaterally to the contact side.

The results reveal a strong correlation between the sensitivity hierarchy of each zone and its optimal friction level, establishing the necessity for spatially graded texture design. Given that the efficacy of friction modulation typically amplifies with the number of texture units interacting with the interface[35, 37], the areal density of the textures was modulated to match the relative magnitude of the optimization targets in each zone. Based on this principle, the friction gradient distribution was formulated as follows (illustrated in Fig. 7):

Inner Roller (Density: F > E) : To achieve the maximum friction level in the Primary Sensitive Zone (Zone F), a high-density array of crater-like features (represented by solid circles in Fig. 6a) was applied to maximize mechanical interlocking. This dense region comprises 30 concentric rows with a circumferential pitch of 1 mm and a radial angular pitch of 3°. For the Secondary Sensitive Zone (Zone E), the texture density was reduced to target a moderate friction level; this sparse region consists of only 5 concentric rows with a circumferential pitch of 1 mm and a radial pitch of 2 mm. Notably, this texturing scheme was applied symmetrically to both working flanks of the inner roller profile.

Outer Roller (Density: A > B) : For the outer roller, textures were applied only to the side in contact with the blank. A graded distribution of concave micro-dimples (represented by hollow circles in Fig. 6b) was implemented to facilitate lubrication and debris trapping. Reflecting the design strategy, Zone A was assigned a higher density configuration consisting of 30 rows (circumferential pitch: 1 mm, radial angular pitch: 3°), while Zone B was assigned a lower density configuration of 5 rows (circumferential pitch: 1 mm, radial pitch: 2 mm).

Insensitive Zones (Zones C and D): To minimize manufacturing complexity and enhance efficiency, the friction-insensitive Zones C and D remained untextured.

4.3. Laser Fabrication and Roll Forming Experimental Procedures

4.3.1. Laser Fabrication of Textured Rollers

The rolling dies were fabricated from quenched DC53 steel, a high-strength cold work die steel. The hybrid texturing process was executed using a custom-developed robotic laser machining system. This system integrates a 6-axis robotic arm (M-10iA/8L, FANUC, Japan) for flexible positioning, coupled with two distinct laser sources to achieve specific topographic features: a picosecond fiber laser (MLPS-20, Laize, China) for ablation and a long-pulse fiber laser (RFL-C500, Raycus, China) for melt-texturing.

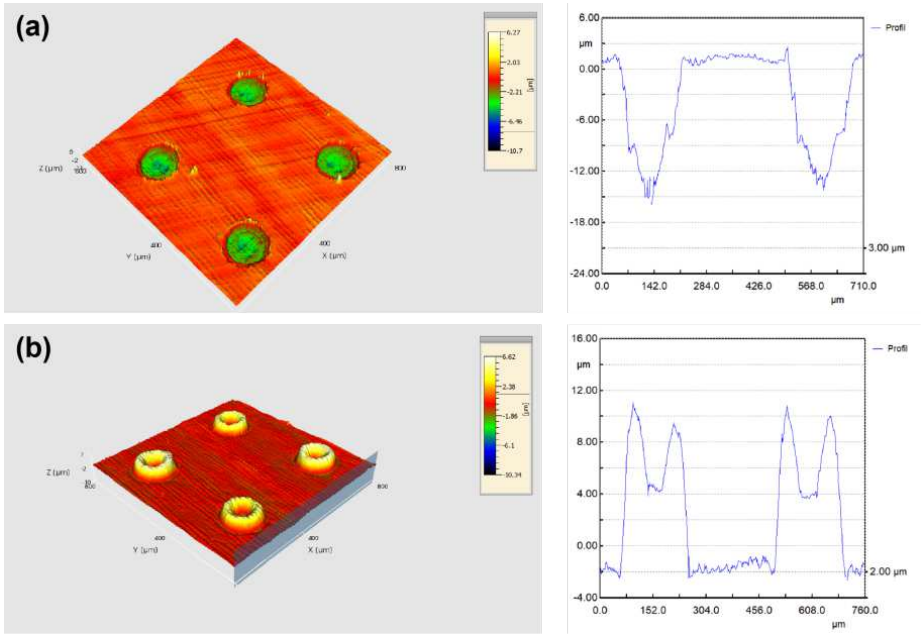


Fig. 8. Surface characterization of the laser-fabricated micro-textures: (a) 3D m

orphology and cross-sectional profile of the concave micro-dimples; (b) 3D mor phology and cross-sectional profile of the convex crater-like micro-textures.

For the friction-reducing zones (A and B), the concave micro-dimples were fabricated using the picosecond laser. The ultrashort pulse width of this laser regime enables cold ablation, where material is rapidly sublimated with minimal thermal diffusion, resulting in clean, burr-free micro-cavities. Based on preliminary process optimization, the machining was carried out under the following optimized parameters using a raster scanning strategy: a laser power of 12 W, a scan speed of 1200 mm/s, 4 scans, and a pulse repetition rate of 500 kHz. The resulting dimple morphology is shown in Fig. 8a.

For the friction-enhancing zones (E and F), the convex crater-like micro-textures were generated using the long-pulse fiber laser. This process relies on a melt-dynamics mechanism, where high-energy, long-duration laser pulses induce a localized melt pool. Driven by surface tension gradients and recoil pressure, the molten material flows radially outward and resolidifies, forming a raised structure. The optimized process parameters were: power of 180 W and a pulse width of 2000 μs. The resulting convex morphology is presented in Fig. 8b.

During fabrication, the rollers were mounted on a positioning worktable (see Fig. 9a). The robotic arm dynamically manipulated the laser processing head to ensure normal incidence of the laser beam relative to the curved roller surface at all processing points (see Fig. 9b). The graded areal density designs (1 mm / 3° for primary zones, 1 mm / 2° for secondary zones) were precisely executed by the CNC program. It is noteworthy that the spatial gradient strategy (i.e., the distribution of high vs. moderate density relative to sensitivity zones) is topologically consistent for both the inner and outer rollers; therefore, the inner roller is presented here as a representative demonstration. As shown in Figure 9c, the variation in texture density across the zones on the processed inner roller is visibly evident, indicating that the gradient design strategy was successfully implemented.

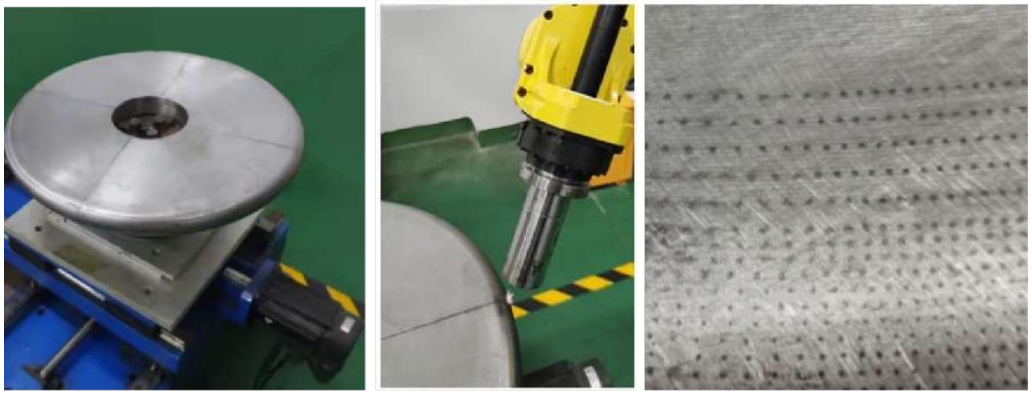


Fig. 9. Experimental setup for the robotic laser texturing process: (a) The large-scale die secured on the positioning worktable; (b) Robotic laser processing ensuring normal beam incidence relative to the curved surface; (c) Optical macro-graph of the fabricated gradient textures on the die surface.

The roll forming experiments were conducted on WS-8 large-diameter bellows forming machine (Boge Dongjin Pipeline Equipment Co., Ltd., China). To ensure strict comparability with the numerical model established in Section 3.1, the experimental process parameters were identical to those used in the simulation. Specifically, the rotational speed of the tubular blank was set to 1.5 rad/s, and the inner roller executed a radial feed motion at a constant velocity of 0.3 mm/s until a total infeed depth of 50 mm was achieved. During the forming process, a commercial lubricating oil (M68) was applied to the tool-workpiece interface. Comparative trials were carried out using two distinct die configurations: the conventional untextured rollers (baseline) and the laser textured rollers (optimized). For each configuration, the forming process was repeated three times to verify the stability of the process and the reproducibility of the results.

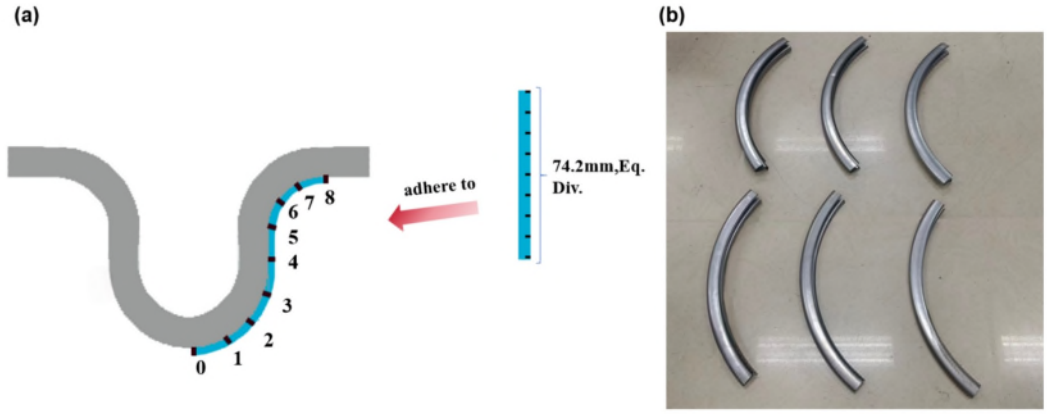


Fig. 10. Methodology for wall thickness characterization: (a) Schematic illustration of the sampling points (0-8) defined by a custom flexible scale based on the unrolled CAD profile (Total arc length: 74.2 mm). (b) Physical arc-shaped specimens extracted via WEDM; the top row displays samples formed by the conventional tooling, while the bottom row displays samples formed by the hybrid textured rollers.

To precisely characterize the wall thickness evolution, a destructive testing method was employed using Wire Electrical Discharge Machining (WEDM). This non-contact cutting technique was chosen to segment the formed bellows along the radial direction (as shown in Fig. 10b) without inducing secondary plastic deformation or geometric distortion. To ensure high-precision localization along the complex curved profile, a custom flexible adhesive scale was fabricated based on the unrolled geometry from the CAD model. The exact meridian arc length of the sampling section was determined to be 74.2 mm. Accordingly, a scale was prepared with nine detection points (labeled 0 to 8) pre-marked at equidistant intervals. This scale was then adhered to the outer surface of the physical specimens, aligning the start and end points with the crest apex and sidewall inflection respectively, to accurately transfer the sampling coordinates onto the outer wall. Subsequently, the wall thickness at each designated point was measured using a high-precision digital point micrometer (Resolution: 0.001 mm). The use of a point-contact anvil was strictly enforced to eliminate geometric errors caused by the curvature of the wave crests and roots. To mitigate random errors and ensure data reliability, measurements were repeated three times at each location, and the arithmetic mean was calculated as the final value.

5. Results and Discussion

5.1. Experimental Validation of the Friction Design Strategy

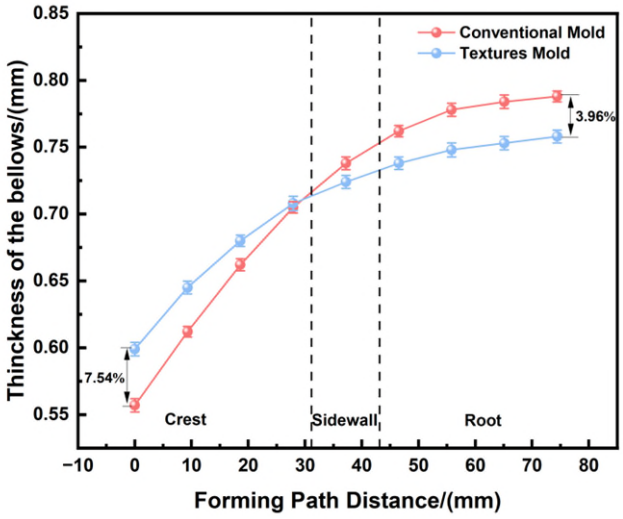


Fig. 11. Comparison of experimental wall thickness profiles.

Fig. 11 presents a comparative analysis of the experimental wall thickness profiles measured along the forming path (from crest apex to root). A direct comparison of the experimental profiles reveals a distinct and significant performance enhancement achieved by the hybrid textured rollers. To elucidate this material redistribution process, the analysis is deconstructed into three characteristic zones along the path:

Zone I: Crest (0-31.1 mm): This region represents the critical deformation zone subject to severe biaxial tension. The textured tooling demonstrates its primary engineering success here by achieving thickness reinforcement. As illustrated in Fig. 10, the minimum wall thickness at the apex (X = 0) increased from 0.557 mm (conventional rollers) to 0.599 mm (textured rollers), representing a substantial net gain of 7.54%. Although the absolute increment appears subtle in magnitude, this percentage increase translates into significant improvements in the fatigue life and pressure-bearing capacity of thin-walled components.

Crucially, a pivotal crossover phenomenon is observed near the distal boundary of this zone (approximately X ≈ 30 mm), where the thickness curves intersect. This intersection point signifies the plastic flow equilibrium where the material-preserving effect of the inner roller's pinning texture is balanced by the material-feeding effect of the outer roller's replenishment texture. The early onset of this crossover confirms that the material compensation mechanism is activated immediately following the crest region.

Zone II: Sidewall (31.1-48.1 mm): This section marks the transition in material flow dynamics, playing a vital role in mass transport and contribution. Unlike the crest apex, the textured profile here (blue line) falls below the conventional baseline (red line). This inversion indicates that the sidewall is not merely a passive bridge but

actively participates in the supply chain. By reducing the frictional drag on the outer surface, the textured roller facilitates the mobilization of material originally residing in this straight section. Consequently, the reduced thickness confirms that the sidewall acts as an efficient transfer conduit, contributing its own material mass to the upward flow towards the crest rather than accumulating it locally.

Zone III: Root (48.1-74.2 mm): The distal region functions as the primary material entry zone, characterized by a sacrificial behavior. The textured roller produces a leaner profile, culminating in a wall thickness of 0.758 mm at the root (X = 74.2 mm), which is 3.96% lower than the 0.788 mm observed for the conventional tooling. This reduction is not a defect but rather a clear validation of successful material reallocation. Whereas the conventional tooling exhibits excessive material accumulation in this non-critical zone, the textured roller effectively redeploys this surplus material to reinforce the vulnerable crest.

Overall Improvement in Formability: This targeted redistribution of material—sacrificing negligible thickness in the robust root section to strategically reinforce the critical crest—directly translates to a marked improvement in overall formability. Consequently, the wall thickness uniformity index (U), calculated from the experimental data, was enhanced from 0.707 (0.557/ 0.788) to 0.790 (0.599 / 0.758), achieving a relative enhancement of 11.74%.

5.2. Mechanistic Discussion on Synergistic Material Flow Control

1. The Replenishment Mechanism: Flow Promotion via Friction Reduction

The interface between the outer roller and the tubular blank serves as the critical pathway for material inflow into the deformation zone. In conventional processes, high friction at this interface constitutes the primary resistance to flow. By introducing concave micro-dimples, this contact surface is effectively transformed into a low-resistance conduit. These micro-dimples not only trap abrasive debris to maintain surface integrity but also function as micro-reservoirs for lubricants, inducing a secondary lubrication effect under heavy loads. This tribological improvement significantly reduces drawing resistance, allowing material from the outer diameter to slide more freely into the forming zone, thereby actively replenishing the wave crest region undergoing severe tensile thinning.

2. The Anchoring Mechanism: Flow Suppression via Friction Enhancement

The meshing of the inner roller with the crest's inner surface is decisive for final wall thickness. The high-density crater-like textures introduced at this interface exert a potent braking function. The raised, hardened asperities generate substantial tangential shear resistance through the dual physical effects of mechanical interlocking and micro-ploughing. This robust constraint effectively counteracts the natural tendency of the material to slip under biaxial stretching, firmly anchoring the material in situ at the crest, thus preventing excessive thickness dissipation.

3. Spatiotemporal Synergy and Targeted Intervention

The efficacy of this strategy stems from the spatiotemporal synergy of the aforementioned mechanisms. It is the dynamic equilibrium established between active external supply and synchronous internal retention that enables the fundamental improvement in wall thickness uniformity. Furthermore, the gradient texture

distribution embodies the principle of targeted intervention: maximizing texture intensity (densest dimples and craters) in the Primary Sensitive Zones (Zones A and F) addresses the critical conflicts, while applying moderate texture density in Secondary Sensitive Zones (Zones B and E) offers a sub-optimization that balances control requirements with manufacturing cost-effectiveness.

4. Summary: From Passive Adaptation to Active Design

Fundamentally, this work signifies a paradigm shift from the passive, uncontrolled material redistribution inherent in traditional forming to active, engineered material precision allocation. This transition is achieved by redefining friction, not as a nuisance property to be globally minimized, but as a spatially tailorable design parameter. By strategically deploying this parameter to precisely steer material flow, defect susceptibility is reduced, ultimately enhancing the structural integrity of high-performance bellows.

6. Conclusions

To address the persistent challenge of severe crest wall thinning in the roll forming of large-scale metallic bellows, this study proposed an active material flow control strategy based on simulation-guided spatially modulated friction. Through high-fidelity finite element modeling, zonal sensitivity analysis, and the fabrication of hybrid laser-textured tooling, the engineering feasibility and effectiveness of this approach were systematically validated. The main conclusions are drawn as follows:

1. **Mechanisms of Spatially Modulated Friction on Material Flow**: Numerical simulations revealed that friction conditions in distinct contact zones exert divergent influences on wall thickness evolution. High friction in the inner roller contact zones (specifically Zones E/F) induces a significant pinning effect, effectively suppressing the tangential outflow of material from the wave crest. Conversely, low friction in the outer roller contact zones (specifically Zones A/B) significantly reduces drawing resistance, promoting replenishment flow from the exterior into the deformation zone. This differential inner-resisting and outer-feeding friction distribution serves as the physical basis for quality enhancement.

2. **Hierarchical Classification of Zonal Sensitivity**: Based on the significant differences in the weight of influence on forming quality, a Primary-Secondary-Insensitive three-level evaluation system was established. The Primary Sensitive Zones (Zones F and A) play a decisive role in wall thickness control, while the Secondary Sensitive Zones (Zones E and B) serve an auxiliary regulatory function. Notably, the Insensitive Zones (Zones C and D) exhibit marked frictional inertia. This finding offers a vital insight for cost-effectiveness: surface modification need not be globally applied but can be strategically focused only on key sensitive regions.

3. **Engineering Realization via Hybrid Laser Texturing**: A fabrication strategy based on heterogeneous laser processing was proposed and verified, achieving the effective physical translation of simulation-designed friction strategies onto the tooling surfaces. Long-pulse laser irradiation was used to induce crater-like asperities in friction-enhancing zones to reinforce mechanical interlocking, while picosecond laser pulses were employed to fabricate micro-dimples in friction-reducing zones to act

as micro-reservoirs. These experiments demonstrate the feasibility of constructing functionally graded friction fields on complex curved die surfaces.

4. **Quantifiable Enhancement of Forming Quality**: Comparative roll forming experiments demonstrated that, relative to conventional smooth dies, the textured tooling achieved a significant optimization in wall thickness distribution. The minimum wall thickness at the wave crest increased by 7.54%, and the overall wall thickness uniformity improved by 11.74%. This improvement validates a targeted material reallocation strategy—sacrificing negligible thickness in the robust root to strategically strengthen the critical crest. These results confirm the spatiotemporal synergy of the anchoring and replenishment mechanisms, effectively surpassing the precision limits of traditional uniform-friction processes.

In summary, this study validates hybrid laser texturing as a robust engineering approach for spatially modulating die friction. By enabling a cost-effective manufacturing strategy that concentrates intervention exclusively on sensitive zones, this approach achieves a targeted material reallocation—strategically sacrificing the non-critical root to reinforce the vulnerable crest. Ultimately, this work redefines friction from a passive disturbance factor in traditional processes to an active, spatially tunable design parameter, establishing a promising technological paradigm for the precision forming of complex components.

Declarations

Funding

This work was supported by the National Natural Science Foundation of China (Grant No.52075225).

Conflicts of interest/Competing interests

The authors have no relevant financial or non-financial interests to disclose.

Availability of data and materials

The datasets generated and/or analysed during the current study are available from the corresponding author on reasonable request.

Authors' contributions

Hao Fu: Conceptualization, Methodology, Funding acquisition, Supervision, Writing. **Jialin Qu:** Methodology, Software, Investigation, Writing - Original Draft. **Hangcheng Zhang:** Software, Validation, Data Curation. **Tianyu Shan:** Validation, Formal analysis. **Shuqian Wu:** Resources. **Jingjing Zhang:** Formal analysis. **Hexing Li**: Data Curation. **Yuyang He:** Investigation, Visualization. **Yanhu Zhang:** Conceptualization. **Jinghu Ji:** Validation. **Yonghong Fu:** Supervision, Project administration.

References

[1] Fu P, Yu G, Yang S, et al. Influence of Structural Parameters on the Mechanical

Performance of Multi-Layer U-Shaped Metal Bellows[J]. Metals, 2024, 14(12): 1431.
[2] Gao Y, Wei Y, Liu X, et al. Stress interaction analysis and mitigation in multi-process bellows manufacturing using continuous finite element simulation[J]. Journal of Materials Processing Technology, 2025, 339: 118826.
[3] Sreenivas A, Abeyrathna B, Rolfe B, et al. Longitudinal strain and wrinkling analysis of variable depth flexible roll forming[J]. Journal of Manufacturing Processes, 2022, 81: 414-432.
[4] Wei Z, Cao J, Cheng J, et al. Precise local deformation control for UHSS thin-walled component in roll forming[J]. Journal of Manufacturing Processes, 2024, 112: 302-312.
[5] Lee S W. Study on the forming parameters of the metal bellows[J]. Journal of Materials Processing Technology, 2002, 130: 47-53.
[6] Wang M, Yan M, Yang C, et al. A study on the evolution mechanism of small diameter thin-walled stainless steel bellows during a bending process[J]. Engineering Failure Analysis, 2023, 152: 107462.
[7] Albrecht H, Roland W, Fiebig C, et al. Multi-dimensional regression models for predicting the wall thickness distribution of corrugated pipes[J]. Polymers, 2022, 14(17): 3455.
[8] Huang T, Jiang Y, Qiao M, et al. Influence of Key Material Parameters and Loading Path on Fatigue Failure Behaviors of Corrugated Tubes[J]. JOM, 2024, 76(4): 1973-1983.
[9] Wang Q, Chu G, Sun L, et al. Numerical and experimental study on axial hydroforging process of 5A03 aluminium alloy S-shaped bellows[J]. International Journal of Advanced Manufacturing Technology, 2023, 127(9): 4413-4428.
[10] Yuan Z, Huo S, Ren J. Mathematical description and mechanical characteristics of reinforced S-shaped bellows[J]. International Journal of Pressure Vessels and Piping, 2019, 175: 103931.
[11] Gao Y, Li H, Wang M. Multi-scale friction model considering interfacial topography and microstructure in ultra-low-temperature forming[J]. Tribology International, 2025, 204: 110544.
[12] Gao Y, Li H, Zhao D, et al. Advances in friction of aluminium alloy deep drawing[J]. Friction, 2024, 12, 396-427.
[13] Wu L, Zhao C, Starostenkov M D, et al. Investigation on a novel deep drawing process with hydro-pulsating lubrication for cylindrical parts[J]. International Journal of Advanced Manufacturing Technology, 2025, 139(11): 5639-5662.
[14] Shivpuri R, Zhang W. Robust design of spatially distributed friction for reduced wrinkling and thinning failure in sheet drawing[J]. Materials & Design, 2009, 30(6): 2043-2055.
[15] Kalkan H, Hacaloglu T, Kaftanoglu B. Experimental investigation of friction in deep drawing[J]. International Journal of Advanced Manufacturing Technology, 2017, 92(9): 3311-3318.
[16] Lin B T, Yang C Y. Applying the Taguchi method to determine the influences of a microridge punch design on the deep drawing[J]. International Journal of Advanced Manufacturing Technology, 2017, 88(5): 2109-2119.
[17] Ravikumar N, Tamilarasan T R, Rajendran R. Effect of graphene on friction and

wear behavior of friction composite tested against grey cast iron disc alloyed with copper[J]. Carbon Trends, 2021, 3: 100031.
[18] Xu M, Ali S, Kurniawan R, et al. Nanoparticle-based lubrication during machining: Synthesis, application, and future scope- A critical review[J]. International Journal of Advanced Manufacturing Technology, 2025, 136(10): 4141-4174.
[19] Kolawole F O, Kolade O S, Bello S A, et al. The improvement of diamond-like carbon coatings for tribological and tribo-corrosion applications in automobile engines: an updated review study[J]. International Journal of Advanced Manufacturing Technology, 2023, 126(5): 2295-2322.
[20] Zhuang K, Zhu K, Wei X, et al. A dual-stage wear rate model based on wear mechanisms analysis during cutting Inconel 718 with TiAlN coated tools[J]. Journal of Manufacturing Processes, 2024, 126: 24-34.
[21] Jaritngam P, Saetang V, Qi H, et al. Surface polishing of additively manufactured Ti6Al4V titanium alloy by using a nanosecond pulse laser[J]. International Journal of Advanced Manufacturing Technology, 2023, 127(7): 3463-3480.
[22] Primus T, Beránek L, Pitrmuc Z, et al. Laser polishing of additively manufactured 316L stainless steel with different construction angles[J]. International Journal of Advanced Manufacturing Technology, 2022, 121(5): 3215-3228.
[23] Ablyaz T R, Shlykov E S, Muratov K R, et al. Surface characterization and tribological performance analysis of electric discharge machined duplex stainless steel[J]. Micromachines, 2020, 11(10): 926.
[24] Jithin S, Joshi S S. Surface topography generation and simulation in electrical discharge texturing: A review[J]. Journal of Materials Processing Technology, 2021, 298: 117297.
[25] Canbulat O, Bozkurt F. Comprehensive Investigation of Coverage Rates of Shot Peening on the Tribological Properties of 6061-T6 Alloy[J]. Metals, 2025, 15(9): 964.
[26] Yang Z, Zheng J, Zhan K, et al. Investigation on Surface Characteristic and Tribological Behavior of BS960 Steel by Using Micro-shot Peening and Traditional Shot Peening[J]. Journal of Materials Engineering and Performance, 2023, 32(22): 10165-10174.
[27] Z. Wu, H. Bao, Y. Xing, L. Liu, Tribological characteristics and advanced processing methods of textured surfaces: a review[J]. International Journal of Advanced Manufacturing Technology. 2021,114: 1241–1277.
[28] Yan H, Chen Z, Zhao J, et al. Enhancing tribological properties of WS2/NbC/Co-based self-lubricating coating via laser texturing and laser cladding two-step process[J]. Journal of Materials Research and Technology, 2020, 9(5): 9907-9919.
[29] Basha D N, Samuel G L, Bathe R. Enhancing tribological performance of gray cast iron by laser surface texturing of micro-grooves and micro-crosshatches[J]. Journal of Materials Engineering and Performance, 2025, 34(11): 9878-9887.
[30] Basha D N, Samuel G L, Bathe R. Femtosecond laser surface textured micro-crosshatch patterns for tribological enhancement of gray cast iron[J]. International Journal of Precision Engineering and Manufacturing-Green Technology, 2026, 13(1): 77-87.
[31] Zhang J, Fu Y, Chen T, et al. Laser-induced concave/convex micro-textures array

for enhancing performance of surface coatings: Bond coating in thermal barrier coating system[J]. Journal of Manufacturing Processes, 2024, 117: 232-243.
[32] Qian Y, Jiang M, Zhang Z, et al. On the transformation between micro-concave and micro-convex in nanosecond laser ablation of a Zr-based metallic glass[J]. Journal of Manufacturing Processes, 2021, 68: 1114-1122.
[33] Joshi S S, Sharma S, Mazumder S, et al. Solidification and microstructure evolution in additively manufactured H13 steel via directed energy deposition: Integrated experimental and computational approach[J]. Journal of Manufacturing Processes, 2021, 68: 852-866.
[34] He Y, Yang J, Wang H, et al. Micro-dimple and micro-bulge textures: Influence of surface topography types on stick–slip behavior under starved lubrication[J]. Applied Surface Science, 2022, 585: 152501.
[35] Yang J, Fu H, He Y, et al. Investigation on friction and wear performance of volcano-shaped textured PVD coating[J]. Surface and Coatings Technology, 2022, 431: 128044.
[36] Z. Gong, D. Yang, Y. Yuan, J. Gu, X. Jin, H. Fu, et al., Laser-induced biomimetic microgrooves for friction driving enhancement of piezoelectric motors[J]. International Journal of Precision Engineering and Manufacturing - Green Technology, 2025, 12: 1675–1697.
[37] Y Wang, X Q Zhu, Q Wang, et al.Research on multi-roll roll forming process of thick plate[J]. International Journal of Advanced Manufacturing Technology, 2019, 102(1-4): 17-26.
[38] Yang J, Fu H, Fu Y, et al. Effects of micro dimple's topography parameters on wear resistance of laser textured alcrn coating under starved lubrication condition[J]. Surface Topography: Metrology and Properties, 2021, 9(4): 045005.